Original Article

A human serum albumin-indocyanine green complex offers improved tumor identification in fluorescence-guided surgery

Yunlong Li[1#], Chun Dai[2#], Zhaolai Hua[2], Lin Xia[2], Yongbin Ding[3], Qiang Wang[4], Marie-Laure Matthey Gié[5,6], Michael Bouvet[7], Huiming Cai[8]

[1]Department of Biomedical Engineering, College of Engineering and Applied Sciences, Nanjing University, Nanjing, China; [2]Department of General Surgery, The People's Hospital of Yangzhong City, Yangzhong, China; [3]Department of General Surgery, Pukou Branch of Jiangsu People's Hospital, Nanjing, China; [4]School of Life Sciences, Jiangsu University, Zhenjiang, China; [5]Department of Thoracic and Endocrine Surgery, University Hospital of Geneva (HUG), Geneva, Switzerland; [6]Department of Surgery, Clinica Moncucco, Lugano, Switzerland; [7]Department of Surgery, University of California, San Diego, CA, USA; [8]Nanjing Nuoyuan Medical Devices Co., Ltd., Nanjing, China

Contributions: (I) Conception and design: Y Li, C Dai; (II) Administrative support: H Cai; (III) Provision of study materials or patients: Y Ding, Q Wang; (IV) Collection and assembly of data: Z Hua, L Xia; (V) Data analysis and interpretation: Y Li, C Dai; (VI) Manuscript writing: All authors; (VII) Final approval of manuscript: All authors.

[#]These authors contributed equally to this work.

Correspondence to: Huiming Cai, MS. Nanjing Nuoyuan Medical Devices Co., Ltd., Ziyun Road No. 18, Nanjing 211514, China.
Email: caihuiming@nuoyuanmedical.cn.

Background: Complete tumor removal is critical for achieving a good prognosis in patients but remains challenging for surgeons. Near-infrared fluorescence-guided surgery (NIRFGS) enables surgeons to accurately localize tumors in real time and facilitates accurate resection. Indocyanine green (ICG) has been approved by the U.S. Food and Drug Administration and the National Medical Products Administration for many years. Although the application of ICG has progressed for a variety of surgeries, there are inherent limitations to ICG, including poor water solubility and photostability, short blood half-life, and aggregation in blood, resulting in poor imaging performance. We found that mixing ICG with human serum albumin (HSA) preoperatively and then injecting it can improve the imaging performance.

Methods: We prepared fluorescent probes by combining ICG with HSA and identified their optimal ratio via *in vitro* absorption measurement and emission spectrum characterization of ICG-HSA complex with different mixing ratios and concentration gradients. Subsequently, under the optimal ratio and clinical simulated concentration, we conducted dynamic change analysis of the fluorescence spectral properties after mixing. We then compared the uptake of ICG-HSA *in vitro* for two different cell types and the imaging performance of different molar ratios of ICG and HSA in mouse models.

Results: Through *in vitro* absorption and emission spectrum characterization of ICG-HSA mixtures with different mixing ratios and concentration gradients, the optimal ratio of the mixture was obtained (ICG:HSA =4:5). Using this ratio, clinical simulated concentration, and mixing, we completed the dynamic change analysis of the fluorescence spectrum properties. The results verified that HSA can improve the dispersion and stability of ICG in aqueous solution, reduce the proportion of free-state ICG, and thus improve the biodistribution. Moreover, the fluorescence performance of ICG was improved. ICG-HSA and ICG uptake in MDA-MB-231 cells and imaging *in vivo* showed that HSA increased the enrichment of ICG in tumor compared to ICG alone ($ICG\text{-}HSA_{fluorescence\ intensity}$ =237.3±10.7 *vs.* $ICG_{fluorescence\ intensity}$ =127.1±10.7). Compared with ICG alone, ICG-HSA provided a clearer tumor boundary and higher tumor-to-background ratio (TBR) ($ICG\text{-}HSA_{TBRmax}$ 3.49±0.56 *vs.* ICG_{TBRmax} 1.94±0.23).

Conclusions: This study suggests that ICG-HSA can achieve higher tumor-to-background contrast with shorter time and can provide an overall superior imaging performance compared to ICG alone, thus exhibiting considerable potential for clinical application.

Keywords: Near-infrared fluorescence-guided surgery (NIRFGS); indocyanine green (ICG); tumor imaging; human serum albumin (HSA)

Submitted Dec 20, 2023. Accepted for publication Jan 18, 2024. Published online Jan 29, 2024.
doi: 10.21037/tcr-23-2338
View this article at: https://dx.doi.org/10.21037/tcr-23-2338

Introduction

Malignant tumors are an increasingly prominent disease globally, with new cases and cancer deaths reaching record numbers of 19.3 and 10 million in 2022, respectively (1). Surgery presently remains the first-line treatment for most tumors and can increase the 5-year survival rate of patients by 10-fold (2). Complete tumor removal is a direct factor affecting prognosis. In traditional surgery, surgeons can use preoperative magnetic resonance imaging (MRI), ultrasound, computed tomography (CT), and other imaging methods to assist in diagnosis and localization (2,3). However, during the operation, surgeons mainly rely on experience to judge the tumor margin, which can contribute to recurrence or even death in about 65% of patients (4-6). Therefore, there is an urgent need for an intraoperative method that can locate tumors in real time and assist surgeons to locate and remove tumors more accurately.

In recent years, near-infrared fluorescence-guided surgery (NIRFGS) has developed rapidly and is able to assist surgeons in locating tumors in real time during surgery (7,8). Indocyanine green (ICG) has been approved by the U.S. Food and Drug Administration (FDA) and the National Medical Products Administration (NFDA) for many years and has become the predominant tracer, being used in 75% of NIRFGS procedures. ICG is tissue structure-specific rather than tumor cell-specific, as it localizes to the tumor via the enhanced permeability and retention (EPR) effect (9-12). Over the past decade, many clinical institutions and research teams have conducted NIRFGS with a greatly improved detection level with the use of navigation equipment (13-15).

However, according to the results observed in a large number of clinical and animal experiments in recent years, as a tumor fluorescent tracer, there remain several issues concerning the use of ICG. (I) One issue is background interference, which is caused by ICG monomers freely diffusing into normal tissues throughout the body (16). (II) Another issue is low utilization, as ICG monomers spontaneously aggregate to form micron-sized particles in blood that are captured by the reticuloendothelial system (RES), which reduces the total quantum yield of fluorescence (17). (III) Finally, ICG is time-consuming, and ICG pharmacokinetics are strongly affected by differences in tissue microstructure and patient characteristics [e.g., liver function (18)], with up to 12 hours needed to produce an adequate tumor-to-background ratio (TBR), increasing the burden on hospitals and patients (19). Due to these limitations, new methods for efficient TBR enhancement need to be developed.

Human serum albumin (HSA) is a naturally occurring endogenous protein in the human body, and studies have shown that HSA in aqueous solution can significantly improve the dispersibility and fluorescence properties of ICG (20,21). HSA has two binding sites to ICG (22), including the hydrophobic pocket at site IIA and the polar cation pocket at site IIIA: the former predominantly binds in a strong hydrophobic interaction manner, while the latter involves dipole-dipole, van der Waals, and hydrogen-bonded weak interaction binding (23-26). According to the literature, HSA used with ICG compounds can be

Highlight box

Key findings

- Compared with Indocyanine green (ICG) injection alone, preoperative ICG and Human serum albumin (HSA) injection can achieve an overall superior imaging performance, including higher tumor-to-background and longer imaging time window.

What is known and what is new?

- Various techniques are employed to locate tumors, yet challenges like poor water solubility and photostability, short blood half-life, and aggregation in blood, resulting in poor imaging performance.
- The optimal molar ratio of ICG:HSA was obtained (ICG:HSA=4:5) and the best tumor imaging performance was obtained at this ratio.

What is the implication, and what should change now?

- This new technology allows physicians to perform quick and precise tumor resection under the guidance of fluorescence. The mixture of ICG and HSA can be used as an alternative to clearer intraoperative localization of tumors.

successfully applied in tumor imaging (27,28). However, a study related to the combined use of ICG and HSA are concerned with their use as raw materials in producing new drugs or nanofluorescent probes, and according to FDA statistics, an average of 12 years is needed for a new clinical drug to progress from development to final market application, with the laboratory research stage requiring about 5 years (29); therefore, the prospects of these innovations being applied in clinical practice in the short-term appear limited. At present, HSA-ICG complexes that retain the prototypical structure of each substance and that can directly be premixed are only used in clinical practice for lymph node tracing (30,31). However, their combined application in tumor imaging remains unexplored, and the optimal ICG-HSA imaging mixture ratio and fluorescence spectrum characteristics have yet to be determined.

In this study, HSA and ICG were mixed to obtain a novel composite tracer. The aims of this study were the following: (I) clarify the fluorescence properties of an ICG-HSA mixture; (II) identify the optimal mixing ratio of ICG and HSA for tumor imaging; and (III) compare the imaging performance of the ICG-HSA composite tracer with that of ICG alone *in vivo*. To our knowledge, this work is the first to examine the application of a new combined tracer composed of HSA and ICG in breast tumor imaging. The objectives of the study were to reduce the fluorescence background of normal tissues caused by free forms of ICG but also increases the enrichment of ICG in tumor. ICG-HSA can obtain a higher TBR in shorter time and offers a superior imaging performance to that of ICG alone, thus demonstrating considerable potential for use in clinic. We present this article in accordance with the MDAR and ARRIVE reporting checklists (available at https://tcr.amegroups.com/article/view/10.21037/tcr-23-2338/rc).

Methods

ICG was obtained from Yichang Pharmaceutical Co., Ltd. (Dandong, China). Female 4-week-old BALB/c nude mice were obtained from GemPharmatech Co., Ltd. (Nanjing, China). Phosphate-buffered saline (PBS), penicillin/streptomycin (pen/strep), and Dulbecco's Modified Eagle Medium (DMEM) were obtained from KeyGEN BioTECH (Nanjing, China). Fetal bovine serum (FBS) was obtained from Zhejiang Tianhang Biotechnology (Huzhou, China). HSA was obtained from Gibco (Thermo Fisher Scientific, Waltham, MA, USA). FLI-10B was a diagnostic equipment suitable for open oncology surgery, provided by Nanjing Nuoyuan Medical Devices Co., Ltd. (Nanjing, China). Fluorescence spectrophotometer was RF-6000, purchased from SHIMADU (Shanghai, China). Ultraviolet visible near infrared spectrophotometer was UV-3600PLUS, purchased from SHIMADU (Shanghai, China).

Preparation and characterization of ICG-HSA

ICG and HSA were mixed at molar ratios of 1:5, 2:5, 4:5, 8:5, and 50:5 with a constant mass of ICG. A Vortex 5 mixer (Scientific Industries Inc., Bohemia, NY, USA) was used to rotate the mixture 60 s (10 levels) until full mixture. The solution molar concentration of each mixture ratio was 5×10^{-4} M and 1.98 mL, and the pure aqueous solution was diluted to 5×10^{-5}, 5×10^{-6}, …., 5×10^{-11} M. The particle size of the ICG-HSA mixture at all concentrations at each ratio was measured one by one using a dynamic light scattering (DLS) instrument. The absorption spectra and emission spectra of all solutions were measured with the same preparation method.

Dynamic fluorescence spectrum of ICG mixed with HSA

(I) The ICG-HSA premixed injection experimental group was created as follows: 280 μL of ICG-HSA (4:5) premixed injection (final ICG concentration of 2×10^{-3} M, which is a conventional clinical injection concentration) was instantaneously injected into 40 mL of 4% HSA solution. (II) The ICG-HSA premixed injection control group was created as follows: 280 μL of ICG-HSA (4:5) injection (final ICG concentration of 2×10^{-3} M) was instantaneously injected into 40 mL of water. (III) The ICG injection experimental group was created as follows: 280 μL of ICG aqueous solution was instantaneously injected into 40 mL of 4% HSA solution. (IV) The ICG injection control group was created as follows: 280 μL of ICG aqueous solution was instantaneously injected into 40 mL of water. In these four groups, injection was instantaneous to ensure that the injection sites highly coincided with the fluorescence spectrum acquisition sites.

Cell cultures

Both MCF 10A (normal breast epithelial cell) and MDA-MB-231(Homo sapiens (human) breast) cells were obtained from Jiangsu KeyGEN BioTECH Corp., Ltd. (Nanjing, China). Both cells were cultured in DMEM medium supplemented with 10% FBS. Both media were

supplemented with 100 IU/mL penicillin and 100 μg/mL streptomycin (KeyGEN BioTECH, Nanjing, China). Cell culture conditions included incubation in 5% CO_2 atmosphere at 37 ℃.

Cellular uptake of ICG-HSA

A total of 2×10^5 cells per well were seeded in 6-well plate until the cells adhered to the wall. Media containing ICG and ICG-HSA (4:5, final ICG concentration 10 μg/mL) were used to culture cells. The medium was removed at 1, 2, 4, and 8 h time points. PBS was used to wash the 6-well plate, and 4% paraformaldehyde was used to fix the cells. This 6-well plate was then stored in the dark. Cells were then photographed and images collected using a high-sensitivity visible near-infrared (NIR) dual-channel fluorescence microscope.

Mouse tumor model

To establish the mouse tumor model, 5×10^6 MDA-MB-231 cells in 100 μL of PBS were injected in the right axilla of BALB/c nude mice. All animal studies were approved by the animal protection committee of Nanjing University (approval No. IACUC-2105007), in compliance with protocols approved by the animal protection committee of Nanjing University for the care and use of animals. Mice were kept in a specific-pathogen-free environment and given free access to sterile water and food. All experiments were completed at Nanjing University. A protocol was prepared before the study with registration in ClinicalTrials (https://clinicaltrials.gov/). Imaging experiments were performed when the tumor volume of the mice reached 200 mm^3. The following formula was used to calculate the tumor volume: $\pi/6 \times \text{length} \times (\text{width})^2$. When the tumor volume was approximately 200 mm^3, the mice were intravenously administered ICG-HSA and ICG (three mice per group). The mice were then anesthetized and imaged using the FLI-10B imaging system at different time points (1, 2, 4, 8, 12, 24, and 48 h) using excitation/emission wavelengths of 785/800 nm.

ICG-HSA metabolism and biodistribution in the tumor and muscle

The mouse tumor model was randomly divided into four groups (n=3), in which mixtures of 50:5, 8:5, 4:5, and 1:0 of ICG-HSA solution (at a final ICG dose of 4 mg/kg) were injected through the tail vein, respectively. Imaging experiments were performed with FLI-10B (Nanjing Noyuan Medical Devices Co., Ltd., Nanjing, China) at 1, 2, 4, 8, 12, 24, and 48 h. All mice were sacrificed at 48 h, after which the organs were extracted and fluorescence intensity measured.

NIR imaging system

When using FLI-10B for imaging, we used a built-in camera with an excitation wavelength of 785 nm, and the instrument could collect fluorescence with an emission wavelength between 800 and 950 nm. The camera had 16 gain options with high sensitivity, and the fluorescence intensity measured under different gains was linearly distributed. Therefore, when the fluorescence intensity of animal was low for an extended period of time, the gain could be increased to solve it. When conducting animal experiments, we obtained four images for each photo, which were white light, fluorescence, fusion, and heat images. After the experiment, the fluorescence images could be quantitatively analyzed using ImageJ software (US National Institutes of Health, Bethesda, MD, USA).

Statistical analysis

The fluorescence intensity of the tumor was calculated by the average value of five points at the center, left, right, upper, and lower parts of the tumor, and the fluorescence intensity of normal tissues was calculated by the average value of five points around the tumor. The average fluorescence intensity of three mouse tumors and normal tissues were then calculated. Linear fitting was assessed with Pearson correlation coefficient (Pearson r) in the original environment. Variability between the different groups were analyzed using the *t*-test.

Results

ICG-HSA characterization

The diameter of ICG–HSA was 5.49±1.51 nm, while the diameter of HSA itself was 5.38±0.92 nm, so the binding of ICG to HSA had little effect on the size of the HSA. The absorption spectra measured by different ratios and concentrations of ICG-HSA solutions are shown in *Figure 1*. In the high-concentration ICG aqueous solution (5×10^{-5} M), the absorption peaks were located at 780 and 707 nm (*Figure 1B*), respectively. The first and second peaks were

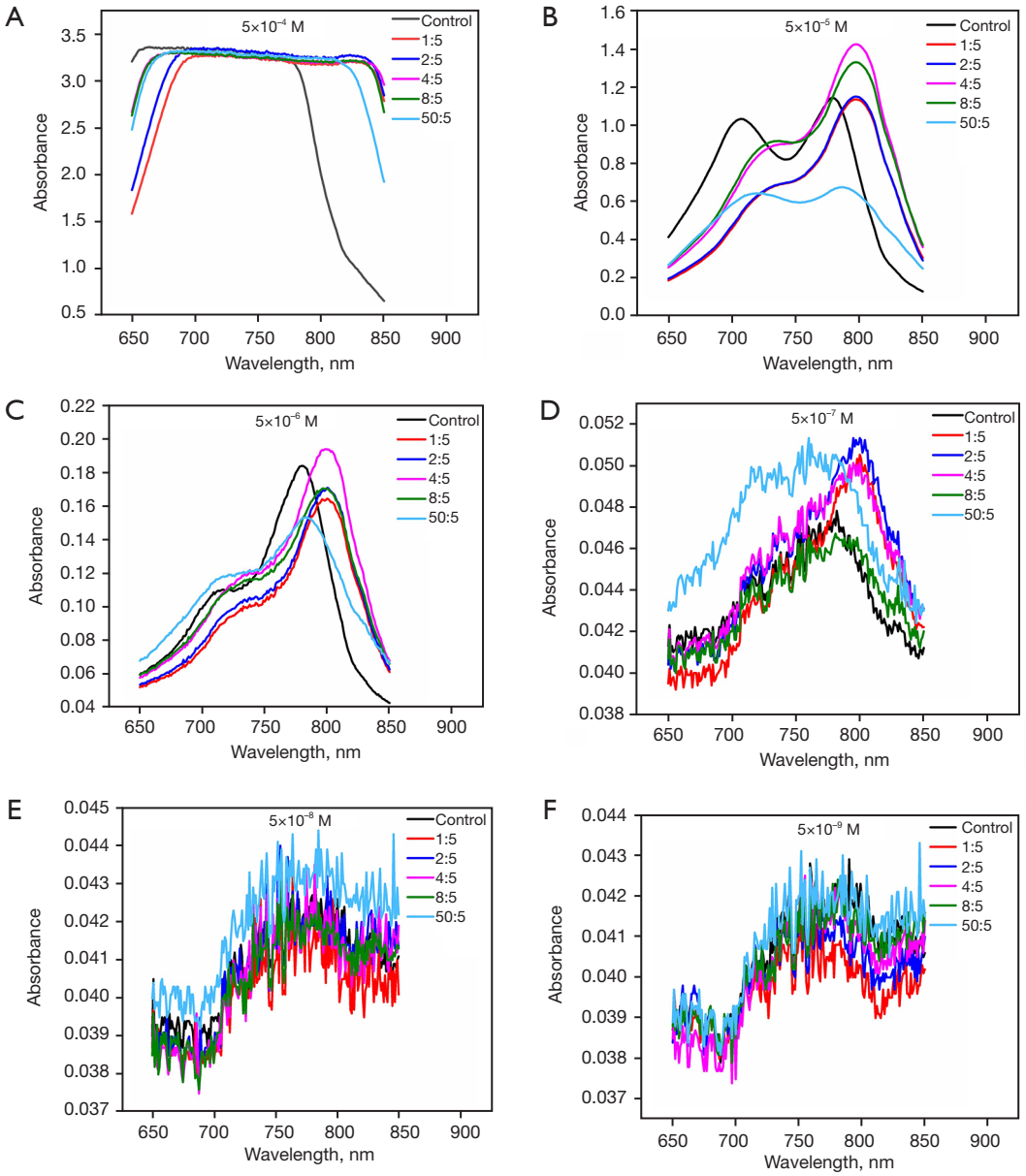

Figure 1 Absorption spectrum determination of ICG and HSA at different concentrations and ratios. (A) ICG concentration of 5×10^{-4} M; (B) ICG concentration of 5×10^{-5} M; (C) ICG concentration of 5×10^{-6} M; (D) ICG concentration of 5×10^{-7} M; (E) ICG concentration of 5×10^{-8} M; (F) ICG concentration of 5×10^{-9} M. ICG, indocyanine green; HSA, human serum albumin.

considered to be monomers and aggregates of ICG; the first peak around 780 nm gradually became dominant, and the second peak around 707 nm gradually decreased or disappeared as the proportion of HSA increased. Similar to the spectral characteristics in aqueous media, we attributed the origin of this secondary peak to ICG aggregation. It can be inferred that the addition of HSA reduces the aggregated forms of ICG. As a result, more ICG molecules absorb NIR light to emit fluorescence, which increases the utilization rate of ICG.

Optimal mixing ratio and concentration of ICG and HSA

In the high-concentration ICG solution (5×10^{-4} to 5×10^{-6} M), the addition of HSA significantly increased the fluorescence intensity and fluorescence intensity integral of the ICG

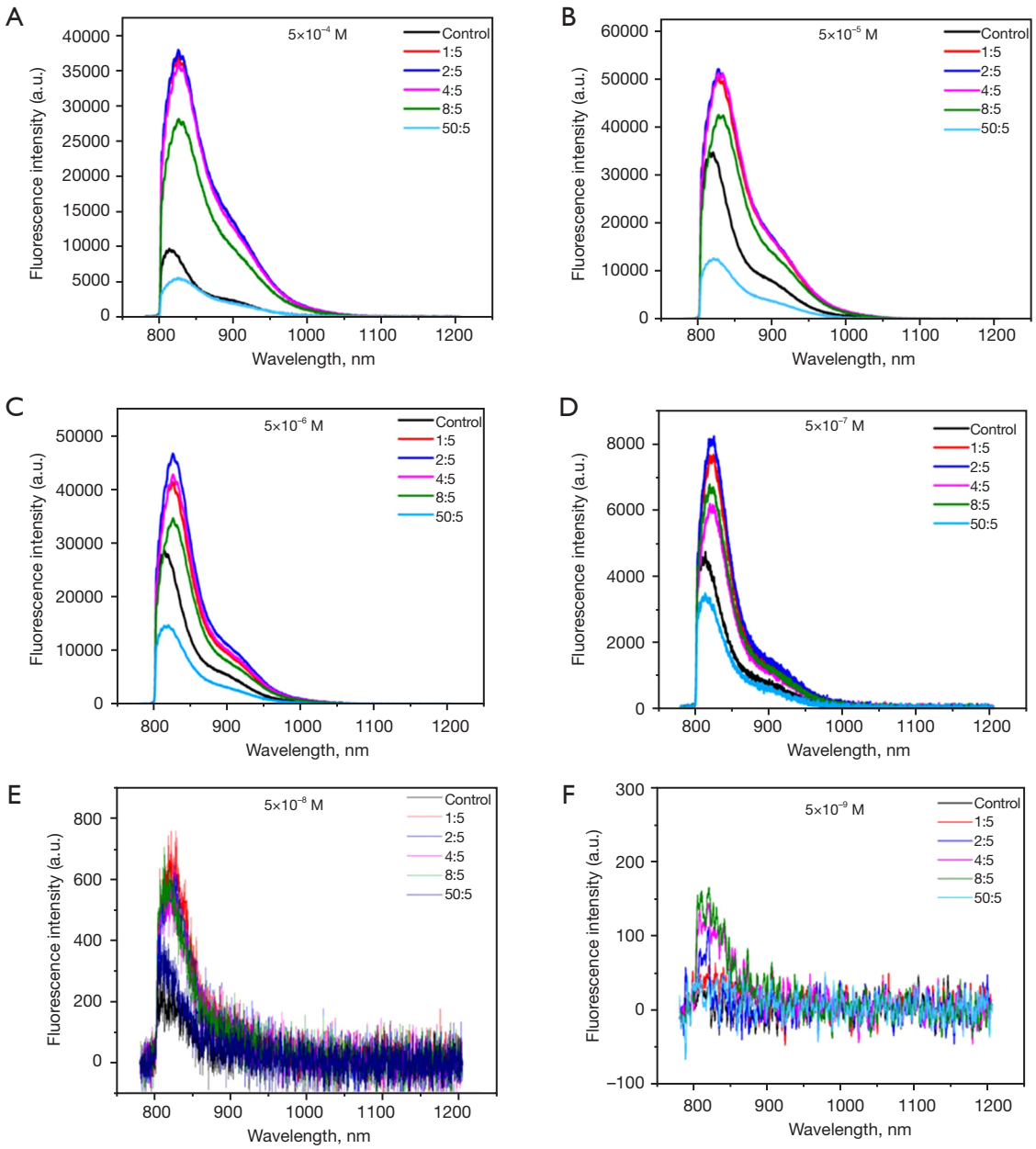

Figure 2 Fluorescence spectrum of ICG and HSA at different concentrations and ratios. (A) ICG concentration of 5×10^{-4} M; (B) ICG concentration of 5×10^{-5} M; (C) ICG concentration of 5×10^{-6} M; (D) ICG concentration of 5×10^{-7} M; (E) ICG concentration of 5×10^{-8} M; (F) ICG concentration of 5×10^{-9} M. ICG, indocyanine green; HSA, human serum albumin.

solution (*Figure 2*). Among the ICG–HSA solution groups, those with 1:5, 2:5, and 4:5 ratios had a better performance, and their fluorescence intensity was the highest, at a concentration of 5×10^{-5} M. This reconfirmed that HSA improves the fluorescence properties of ICG solution via an improvement in the dispersion of ICG monomers. However, the 50:5 ICG-HSA solution hardly contributed to the reduction of ICG aggregation due to the low content of the added HSA; meanwhile, the introduction of larger particles of HSA protein enhanced the scattering of excitation light, hindering the stimulation of the ICG monomer and resulting in a smaller area of fluorescence intensity distribution under the curve than in the control group. The fluorescence integration and fluorescence peak

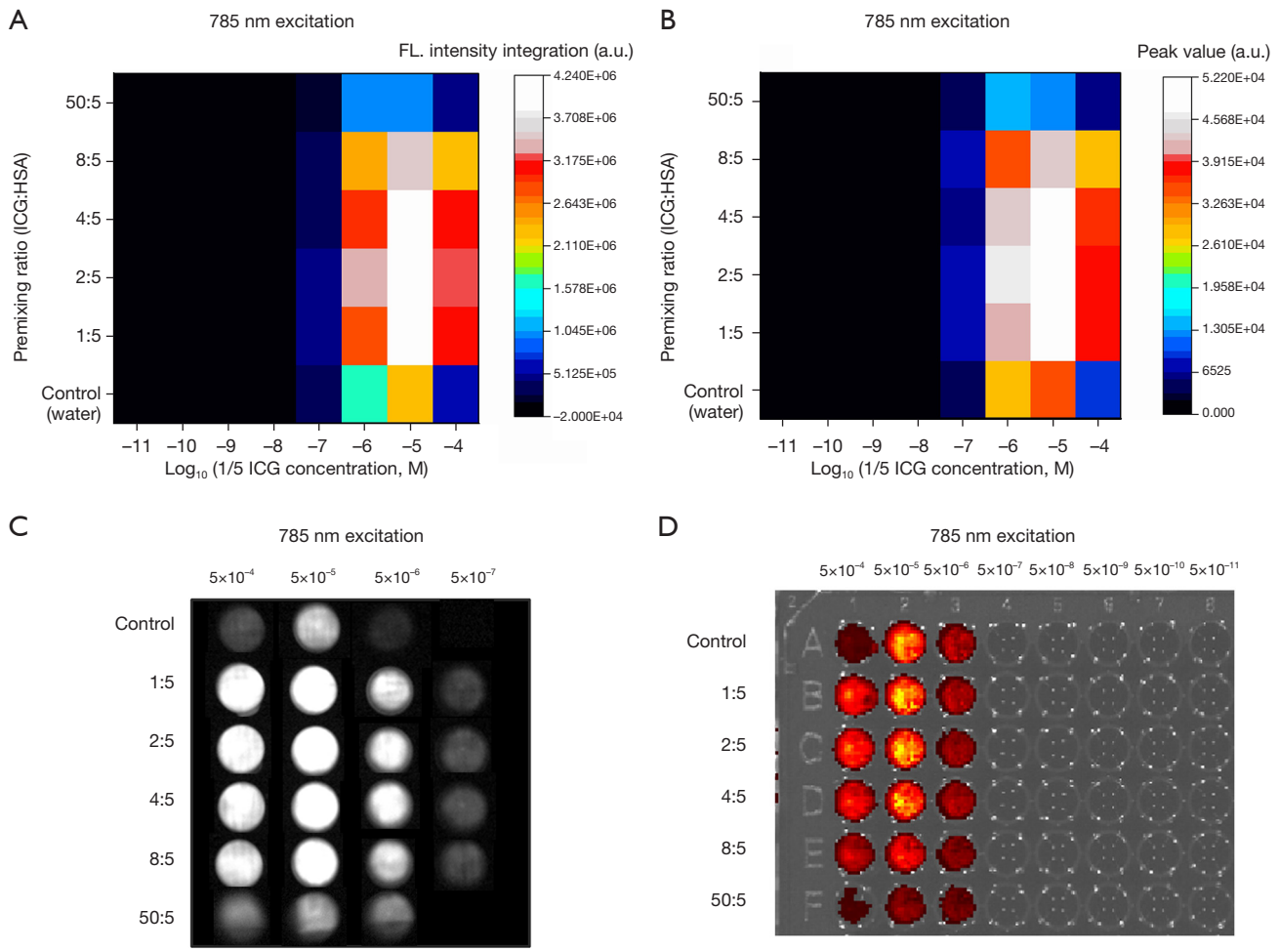

Figure 3 Fluorescence intensity integration and fluorescence peak of ICG and HSA at different concentrations and ratios. (A) Fluorescence intensity integration matrix; (B) fluorescence peak matrix; (C) fluorescence intensity of ICG and HSA complexes at different ratios and concentrations under the FL-10B instrument; (D) fluorescence intensity of ICG and HSA complexes at different ratios and concentrations under the IVIS spectrum. ICG, indocyanine green; HSA, human serum albumin; a.u., arbitrary unit; FL, fluorescence; IVIS, In Vivo Imaging System.

of the ICG-HSA solutions with different mixing ratios and concentrations were plotted in a matrix diagram (*Figure 3*), which showed that the mixing ratios of ICG-HSA with the best fluorescence performance were 1:5, 2:5, and 4:5.

Dynamic fluorescence properties of ICG mixed with HSA

After comprehensive consideration, ICG was mixed with HSA at a ratio of 4:5 and used as the optimal mixing ratio group. In this experiment, the volume of each group of solutions was scaled in equal proportion in strict accordance with the clinical routine injection volume, concentration, and average total blood volume of the human body (*Figure 4A*). According to the dynamic spectrum of instantaneous mixing of ICG and HSA, ICG can rapidly bind and stabilize HSA in solution, and this process can be completed in about 4–8 s (*Figure 4B-4D*). Among the 4 groups, the order of the final concentration of HSA in the solution was as follows: A-a > A-c > A-b > A-d. It could be seen that the fluorescence intensity and stability were positively correlated with the final concentration of HSA in the solution, demonstrating that HSA in the solution could not only improve the dispersity of ICG but also increase its stability in the solution. Considering these three ratios comprehensively, at the dose of 4:5, the absorption value of ICG-HSA complex was the largest, and the fluorescence

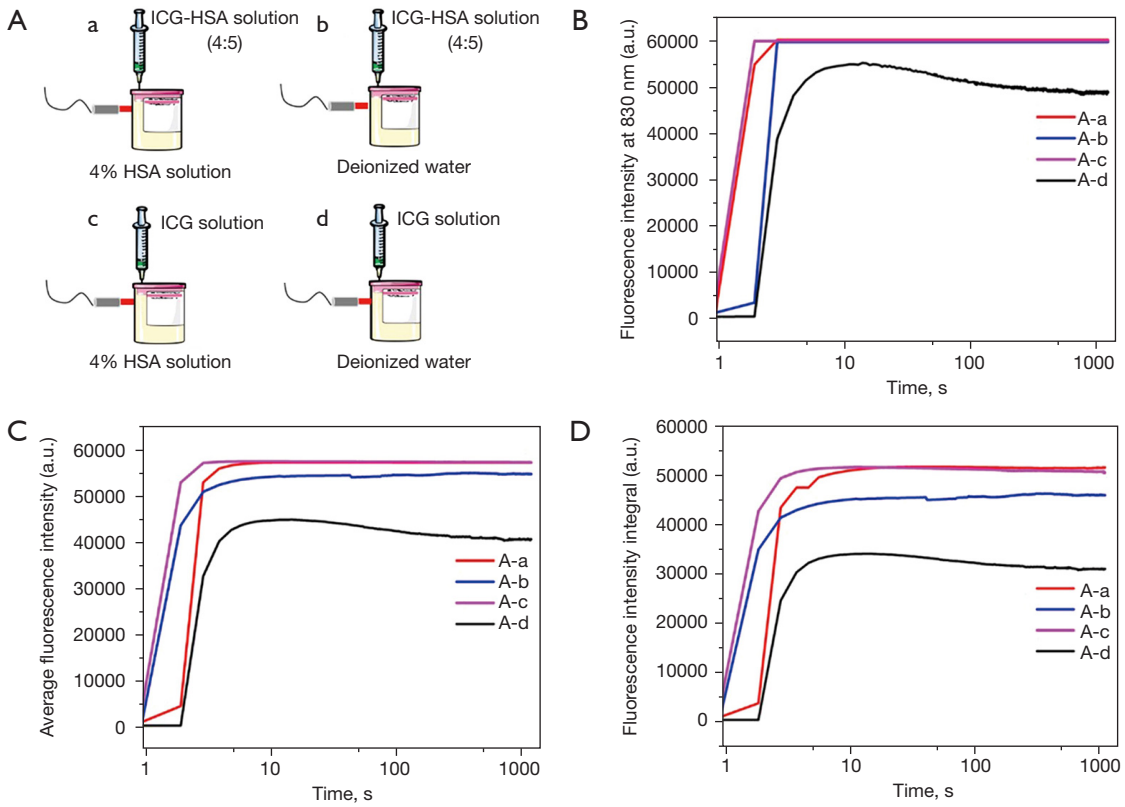

Figure 4 Dynamic time series fluorescence spectrum. (A) Four different transient injection groups; (B) fluorescence intensity at 830 nm over time; (C) mean fluorescence intensity at 800–860 nm over time; (D) fluorescence intensity integral at 800–900 nm over time. A-a: ICG-HSA (4:5) injection was injected into a 4% HSA solution; A-b: ICG-HSA (4:5) injection was injected into deionized water; A-c: ICG solution was injected into a 4% HSA solution; A-d: ICG solution was injected into deionized water. ICG, Indocyanine green; HSA, human serum albumin.

intensity were close, meanwhile, the required HSA dosage was the smallest, so we chose 4:5 ratio to continue research in the subsequent exploration.

Cellular uptake of ICG-HSA and ICG

MDA-MB-231 and MCF-10A cells were cultured with ICG-HSA (molar ratio of 4:5) and ICG for 1, 2, 4, and 8 h, ensuring that the concentration of ICG was 10 μg/mL. The mean fluorescence signal of cells cultured with ICG-HSA was significantly stronger than that of cells incubated with ICG at all time points (*Figure 5*). Both probes were mainly present in the cytoplasm and intercellular space of MDA-MB-231 and accumulated to the peak at 4 h, while they were rarely present in MCF-10A cells, which indicated that the uptake mode of ICG-HSA and ICG by MDA-MB-231 cells was indistinguishable; however, because tumor cells tended to take up protein as an energy supply source, the presence of HSA not only increased the fluorescence intensity in MDA-MB-231 cells but also increased the uptake of ICG-HSA by these cells.

Tumor imaging of ICG-HSA and ICG

Different ratios of ICG-HSA and ICG were premixed and injected into mice via the tail vein (n=3), and the tumor fluorescence intensity of all groups accumulated to a peak within 1 h and then gradually decayed. The tumor fluorescence intensity of mice with different ratios of premixed ICG-HSA was significantly stronger than that of mice injected with ICG alone within 1 h (*Figure 6*). In contrast, the fluorescence intensity of normal tissues in groups with HSA injection was slightly lower than that of the control group (*Figure 7A*, *Table 1*), so ICG-HSA

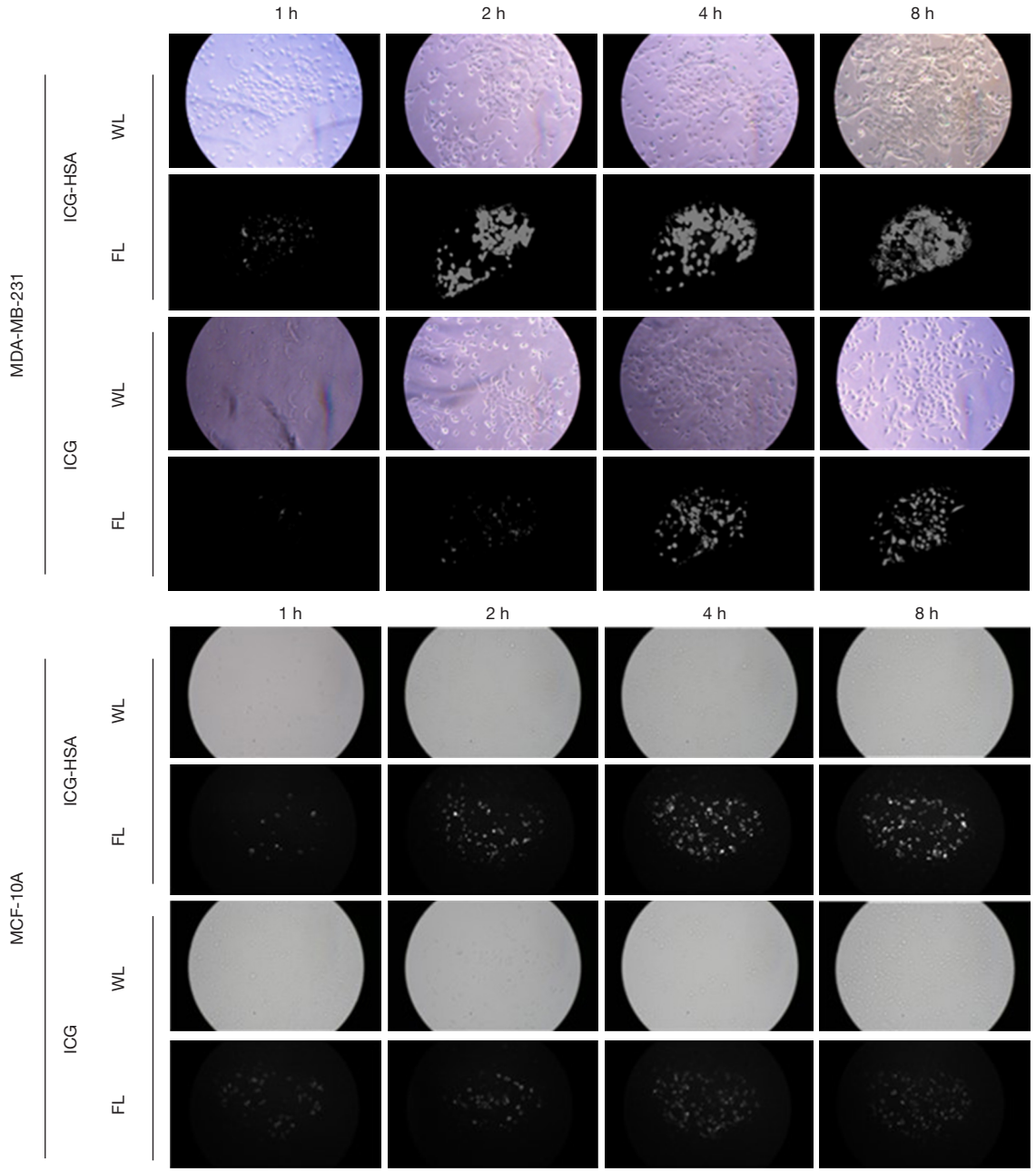

Figure 5 Comparison of cell uptake of ICG-HSA (4:5, final ICG concentration of 10 μg/mL) and ICG between MDA-MB-231 and MCF-10A cell lines (magnification 20×). Medium containing ICG and ICG-HSA (4:5, final ICG concentration 10 μg/mL) were used to culture cells. The medium was removed at 1, 2, 4, and 8 h time points. PBS was used to wash the 6-well plate, and 4% paraformaldehyde was used to fix the cells and images collected using a high-sensitivity visible near-infrared dual-channel fluorescence microscope. ICG, indocyanine green; HSA, human serum albumin; FL, fluorescence; WL, white light.

increased the TBR mainly by increasing the fluorescence intensity of the tumor. Though TBR >1.5 is sufficient to distinguish tumor tissue from non-tumor tissue in fluorescence navigation tumor surgery, higher TBR means better imaging. Compared with ICG alone, 4:5 ICG-HSA has the longest, most stable TBR window and clearest tumor boundary. At the same time, the average TBR of the 4:5 ICG-HSA group was 3.49±0.56, which was

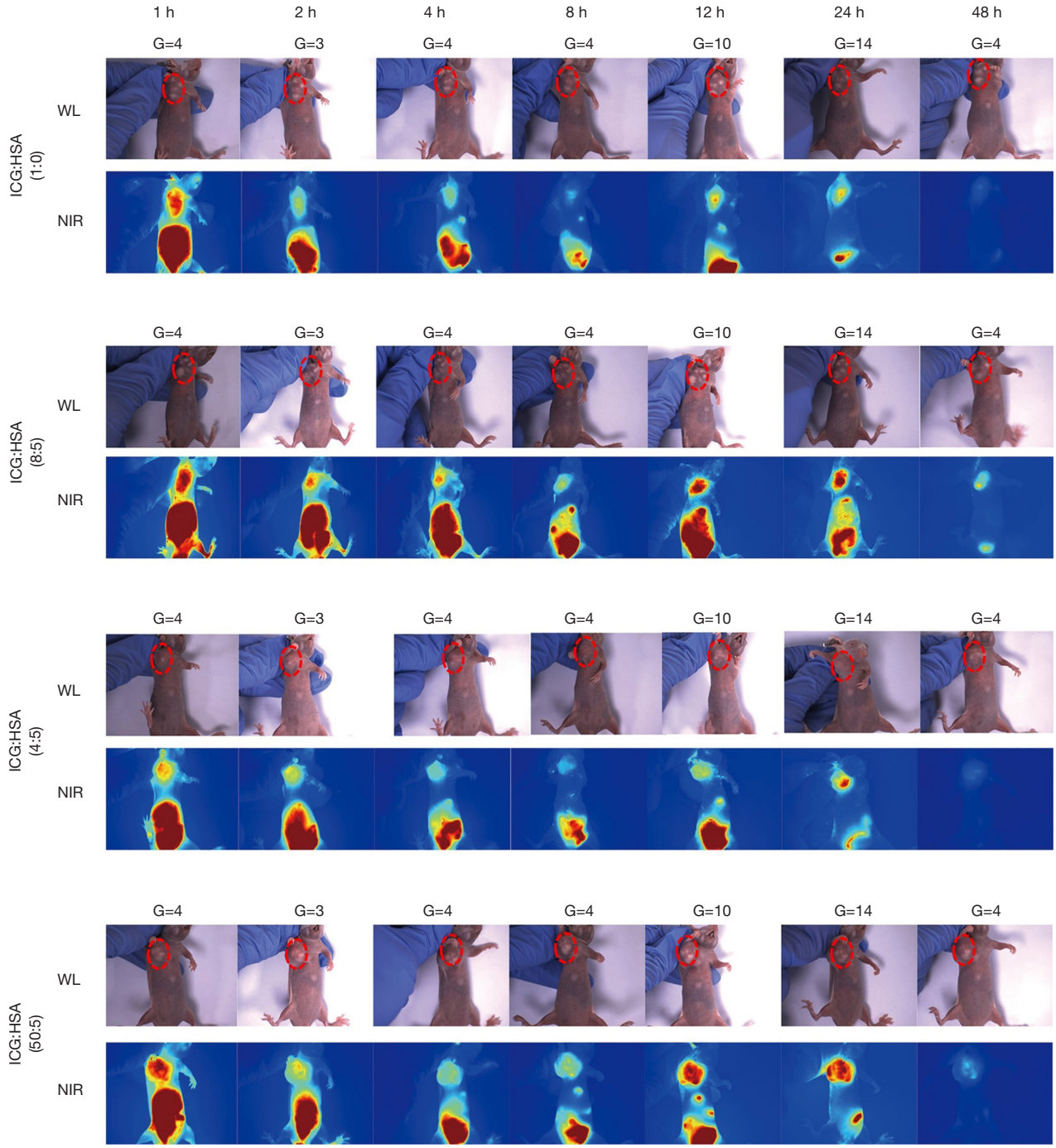

Figure 6 Tumor imaging of ICG and HSA at different concentrations and ratios. The fluorescence intensity measured under different gains is linearly distributed. All animal data are in Figures S1-S4. ICG, indocyanine green; HSA, human serum albumin; G, gain; WL, white light; NIR, near-infrared.

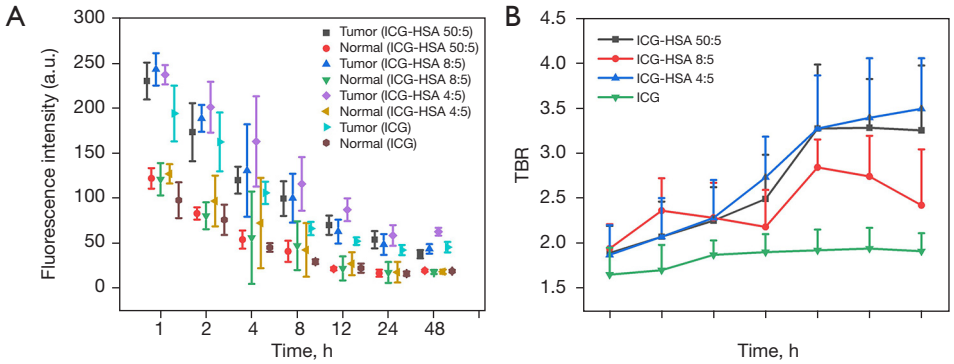

Figure 7 TBR and fluorescence metabolism analysis. (A) The fluorescence intensity curves of tumor and normal tissue with different mixing ratios of ICG and HSA over time; (B) time-dependent curves of TBR under different mixing ratios. a.u., arbitrary unit; ICG, indocyanine green; HSA, human serum albumin; TBR, tumor-to-background ratio.

Table 1 Comparison of fluorescence intensity of tumor and normal tissues at different time points

Time	Fluorescence intensity of tumor				Fluorescence intensity of normal			
	50:5	8:5	4:5	1:0	50:5	8:5	4:5	1:0
1 h	230.3±20.5	243.3±18.0	237.3±10.7	194.2±31.0	122.1±11.4	121.1±18.0	127.1±10.7	97.8±19.9
2 h	173.4±32.3	188.8±15.0	201.2±28.2	162.6±32.7	83.1±6.8	80.5±15.0	96.9±28.2	76.0±16.8
4 h	120.1±15.0	130.8±51.4	163.1±50.2	106.0±12.4	54.0±10.1	56.1±51.4	72.4±50.2	45.3±4.8
8 h	99.6±19.3	100.1±27.1	115.9±29.8	66.3±7.4	41.0±11.7	47.3±27.1	42.5±29.8	29.5±2.6
12 h	70.1±10.7	62.9±13.3	87.2±12.7	52.3±4.2	21.5 ±1.8	22.0±13.3	27.2±12.7	22.3±5.1
24 h	53.9±9.6	48.6±11.6	58.6±11.5	42.4±5.6	16.7 ±4.0	17.5±11.6	17.8±11.5	16.2±2.5
48 h	37.8±4.6	43.7±5.3	62.8±4.4	45.6±5.8	19.5 ±1.3	18.1±2.3	18.3±2.4	19.0±1.4

Data are presented in tables as mean ± standard deviation. 50:5, 8:5, 4:5, 1:0 ratio represents molar ratio of ICG:HAS. ICG, indocyanine green; HSA, human serum albumin.

significantly higher than that of the ICG alone group (ICG-HSA$_{TBRmax}$ 3.49±0.56 *vs.* ICG$_{TBRmax}$ 1.94±0.23, *t*-test; P<0.05) (*Figure 7B*, *Table 2*). In summary, the imaging performance of ICG-HSA was much better than that of ICG for tumor imaging in a short period of time. A higher TBR means that the tumor boundary can be judged more clearly when removing tumors, assisting doctors in accurately removing tumors while retaining more normal tissue.

Discussion

Improvement of dispersion and fluorescence properties of ICG by HSA in solution

When ICG was dissolved in deionized water as a control, the ICG maximum absorption wavelength appeared at 780 nm, which was the dominant feature throughout the concentration range studied (5×10^{-5} to 5×10^{-9} M) (*Figure 1*). At ICG concentrations above 5×10^{-7} M, a distinct secondary peak at approximately 707 nm appeared, and peak value increases with increasing concentration (*Figure 1B,1C*). Philip *et al.* attributed the absorption peaks at 780 and 707 nm to the monomeric and aggregated forms of ICG, respectively (32); Mauerer *et al.* also proved that the origin of this sub-peak is attributed to the aggregation of ICG (33). The addition of HSA to the ICG solution promoted the red shift of the monomeric absorption peak of ICG to 797 nm, and these experimental results are consistent with those reported by other researchers (34). In addition, ICG is an amphiphilic molecule with a propensity to self-aggregate at low micromolar concentrations in water, and premixed with HSA, its hydrophobic group binds to the HSA protein pocket via van der Waals forces, and the long chain of

Table 2 Tumor-to-background ratio at different time points

Time	Tumor-to-background ratio			
	50:5	8:5	4:5	1:0
1 h	1.89±0.30	1.94±0.27	1.87±0.33	1.65±0.30
2 h	2.07±0.39	2.36±0.36	2.07±0.43	1.70±0.28
4 h	2.25±0.37	2.28±0.39	2.28±0.42	1.87±0.16
8 h	2.49±0.49	2.18±0.41	2.73±0.45	1.90±0.20
12 h	3.27±0.71	2.84±0.31	3.27±0.59	1.92±0.23
24 h	3.28±0.54	2.74±0.45	3.39±0.66	1.94±0.23
48 h	3.25±0.72	2.42±0.62	3.49±0.56	1.91±0.20

Data are presented in tables as mean ± standard deviation. 50:5, 8:5, 4:5, 1:0 ratio represents molar ratio of ICG:HAS. ICG, indocyanine green; HSA, human serum albumin.

the hydrophilic group's sulphonate extends externally, reducing the aggregation of ICG molecules and thus increasing the dispersion of the monomer. Experimental results showed that ICG-HSA at a mixing ratio of 4:5 performs best. The effective absorption spectrum function of ICG in solutions containing HSA can be described by the following equation (16):

$$\sigma^{HSA}(\lambda) = f_M^{HSA} \cdot \sigma_M(\lambda) + f_{Agg}^{HSA} \cdot \sigma_{Agg}(\lambda) + \sum_{i=1}^{n} f^{*HSA}_{Mi} \cdot \sigma^{*HSA}_{Mi}(\lambda) \quad [1]$$

Where f_M^{HSA} and f_{Agg}^{HSA} are the corresponding proportions of unbound monomeric and aggregate forms of ICG in this solution containing HSA, $\sigma_M(\lambda)$ is the unbound ICG monomer's absorption cross-section, $\sigma_{Agg}(\lambda)$ is the unbound aggregate's absorption cross-section, $f_{M_i}^{*HSA}$ is the proportion of ICG monomers associated with HSA, $_i$ represents the amount of monomers associated with HSA (i.e., 1, 2), and $\sigma_{M_i}^{*HSA}(\lambda)$ is the bound ICG monomer's absorption cross-section. Therefore, the absorbance and fluorescence intensity of ICG are related to different ICG forms, including ICG monomers, aggregates, and HSA conjugates (either HSA mixed with ICG prior to injection and/or formed after ICG injection).

Figure 2 and *Figure 3* show the effect of HSA on ICG fluorescence intensity. Irradiated with a 785-nm laser, the ICG-HSA solution's fluorescence intensity with a molar ratio from 1:5 to 8:5 was significantly enhanced compared with that of the ICG aqueous solution, and the observation results were consistent with those reported in other research (35). This can be attributed to the decrease of the aggregation state of ICG. Since 1–2 ICG molecules are noncovalently bound to the hydrophobic core environment of HSA, the binding with HSA brings higher levels of monomers, as well as the gradual decrease of aggregates. After binding to HSA, the movement of ICG is hindered, so that the confined molecular vibration and translation of ICG can minimize its conformational deformation, thereby enhancing its absorption and fluorescence characteristics (32). The fluorescence intensity of the three ratios of 1:5, 2:5, and 4:5 was similar, and the ICG-HSA mixture ratio of 4:5 was the optimal ratio when the amount and cost of are considered. At this optimal ratio (4:5), we explored changes in the dynamic fluorescence properties during the mixing of ICG and HSA. The values of each solution volume were scaled in strict accordance with the clinical routine injection volume and the average human blood volume (*Figure 4A*). In the HSA solution environment, ICG could rapidly bind to it and form a steady state, and this process required only 4–8 s (*Figure 4*). Compared with that of the ICG aqueous solution control group without HSA, the fluorescence intensity of the HSA experimental group showed a significant increase and had better stability, indicating that HSA also increased its stability in the solution while enhancing the dispersion of ICG monomers.

Advantages of ICG-HSA in tumor cell uptake

By non-covalently combining ICG with HSA and exploring their optimal mixing ratio, an optical imaging probe of ICG-HSA (mixing ratio of 4:5) was developed and validated in this study. Compared with ICG, the probe has higher stability, fluorescence signal, and relative fluorescence quantum yield (*Figure 5*). Moreover, it has been reported that tumors break down HSA into amino acid components that serve as their energy source for accelerated growth (36).

In addition, the HS-binding protein receptor-mediated has uptake pathway is also involved, including the membrane-associated 60-kDa glycoprotein and the secreted protein, acidic and rich in cysteine (SPARC) (37). Researchers have found that SPARC is overexpressed in human breast cancer compared to healthy breast tissue (38,39), resulting in higher uptake of ICG-HSA by MDA-MB-231 cells. Therefore, ICG-HSA not only has the advantages of enhancing the dispersion and fluorescence properties of ICG monomers but also has extraordinary advantages in tumor cell uptake.

Advantages of ICG-HSA in tumor imaging

HSA can combine with ICG to form nanoparticles of about 4–7 nm in size, thereby reducing the number of ICG free monomers and avoiding the background interference caused by their free diffusion; meanwhile, this avoids wasting the ICG captured by the human RES due to the formation of aggregates (17), Thus, it is enriched in tumor tissue through blood circulation and EPR effect (9,40,41), achieving better tumor imaging effect, which greatly improves the utilization rate of ICG and optimizes its imaging performance (*Figure 6*). All animal data are in Figures S1-S4. This paper is the first to report the mixing of an ICG and HSA prototype for tumor imaging. After mixing ICG and HSA in different ratios, exploring their optimal tumor imaging mixing ratio, and assessing the value and stability of TBR and tumor boundary definition, we identified 4:5 ICG-HSA to be the optimal imaging mixing ratio ($ICG\text{-}HSA_{TBRmax}$ 3.49±0.56 *vs.* ICG_{TBRmax} 1.94±0.23, *t*-test; P<0.05). HSA improves its fluorescence performance by increasing the dispersion and stability of ICG, reduces the fluorescence background interference caused by free-form ICG, and increases the perfusion of ICG to tumors by increasing the monomeric forms of ICG, thus obtaining a higher TBR and a clearer tumor boundary (*Figure 7*).

ICG-HSA has been reported for lymph node mapping. Hutteman *et al.* used a perimammary injection of 1.6 mL of 500-μM ICG aqueous solution and ICG-HSA composite solution for sentinel lymph node detection in patients with breast cancer. Their study showed that there was no significant difference in signal-to-background ratio (SBR) between the ICG-HSA group and the ICG group (8.4±3.6 *vs.* 11.3±4.8; P=0.18), so there was no direct benefit of premixing ICG and HSA before injection for breast cancer (39). However, no study has been reported on preserving the prototype of both ICG and HSA for tumor imaging, and related studies used derivatives of ICG and HSA or nanofluorescent probes for tumor fluorescence imaging (27,28). The imaging effect has been demonstrated to be better than that of traditional ICG imaging, but as a new drug, an extensive period of time and large economic cost from research and development to marketing are required (29). It is therefore difficult to obtain FDA approval of drugs for clinical practice in the short-term. Both the ICG and HSA injection examined in this paper are clinical injection-grade reagents that have been approved by the FDA, and their long-term clinical use has confirmed their biosafety. In addition, in this study, we retained the prototype of the 2 for pre-mixing and did not introduce any other components, which ensured its safety. The results showed that in a short time (within 48 h), ICG-HSA at a mixing ratio of 4:5 had the largest and most stable TBR window and the clearest tumor boundary, which was significantly higher than the ICG imaging performance ($ICG\text{-}HSA_{TBRmax}$ 3.49±0.56 *vs.* ICG_{TBRmax} 1.94±0.23; *t*-test; P<0.05). In summary, ICG-HSA can achieve high-contrast imaging of tumors in a short time and a superior imaging performance to that of ICG, thus demonstrating its considerable potential for clinical translation.

Although the ICG-HSA complex significantly improved the TBR for tumor imaging, it could not fundamentally overcome the limitations of ICG. For example, it does not possess tumor specificity, is metabolized by liver and intestine, and cannot be used for the localization of intestinal tumors. However, the long-term stability of ICG-HSA complex and its application in real-time monitoring of tumor progression may be valuable. Simultaneous investigation of ICG-HSA for visualization of other tumor types would enhance the translational potential. In addition, exploring the use of ICG-HSA in combination with other imaging modalities and the development of tumor-specific NIR-targeted tracers could open up avenues for multifunctional applications in cancer diagnosis and therapy.

Limitations

Due to the complicated protein composition and metabolism process in organisms, the absorption and emission spectral characteristics of various components in the ICG-HSA solution should be systematically and quantitatively investigated and simulated in future research. Additionally, the relatively shallow penetration depth of

fluorescence imaging may restrict it value for assisting with deeper lesion resections. We should thus focus on the application of ICG-HSA for the photoacoustic imaging of tumors to increase the tissue penetration depth to the centimeter level.

Conclusions

In this study, a new composite ICG-HSA fluorescent tracer for injection and its preparation method were proposed to improve the dispersion and fluorescence performance of ICG in aqueous solution, and the optimal ICG-HSA mixing ratio (4:5) was identified. In addition, this is the first report of the ICG-HSA complex being applied to breast cancer imaging, and the results confirm that it has significant advantages over traditional ICG tumor imaging, with shortened surgical waiting time, satisfactory TBR, and wider surgical window. Further exploration is needed in the future to see if the complex can aid in the visualization of other types of tumors. Although the complex is not tumor specific, the enhanced tumor uptake due to the presence of HSA also significantly improves the TBR during imaging of the complex, which is promising for future applications in the visualization of a wide range of tumor types. In addition to having characteristics of high biocompatibility and low toxicity, ICG-HSA will have a streamline clinical approval process. Explorations and innovations related to ICG-based NIRFGS technology in tumor imaging have great potential for clinical translation.

Acknowledgments

Funding: This study was supported by funding from the State Commission of Science & Technology of China (No. 2016YFC0104100), the National Natural Science Foundation of China (No. 81901843), the Fundamental Research Funds for the Central Universities (No. 2022300326), and the Jiangsu University 2023 Medical Education Collaborative Innovation Fund (Nos. JDYY2023144, JDYY2023145, and JDYY2023146).

Footnote

Reporting Checklist: The authors have completed the MDAR and ARRIVE reporting checklists. Available at https://tcr.amegroups.com/article/view/10.21037/tcr-23-2338/rc

Data Sharing Statement: Available at https://tcr.amegroups.com/article/view/10.21037/tcr-23-2338/dss

Peer Review File: Available at https://tcr.amegroups.com/article/view/10.21037/tcr-23-2338/prf

Conflicts of Interest: All authors have completed the ICMJE uniform disclosure form (available at https://tcr.amegroups.com/article/view/10.21037/tcr-23-2338/coif). Huiming Cai is from Nanjing Nuoyuan Medical Devices Co., Ltd. The other authors have no conflicts of interest to declare.

Ethical Statement: The authors are accountable for all aspects of the work in ensuring that questions related to the accuracy or integrity of any part of the work are appropriately investigated and resolved. All animal studies were approved by the animal protection committee of Nanjing University (approval No. IACUC-2105007), in compliance with protocols approved by the animal protection committee of Nanjing University for the care and use of animals.

References

1. Siegel RL, Miller KD, Fuchs HE, et al. Cancer statistics, 2022. CA Cancer J Clin 2022;72:7-33.
2. Global, regional, and national age-sex specific mortality for 264 causes of death, 1980-2016: a systematic analysis for the Global Burden of Disease Study 2016. Lancet 2017;390:1151-210.
3. Fischerova D, Pinto P, Burgetova A, et al. Preoperative staging of ovarian cancer: comparison between ultrasound, CT and whole-body diffusion-weighted MRI (ISAAC study). Ultrasound Obstet Gynecol 2022;59:248-62.
4. Stoia S, Băciuț G, Lenghel M, et al. Ultrasonography techniques in the preoperative diagnosis of parotid gland tumors - an updated review of the literature. Med Ultrason 2021;23:194-202.
5. Lauwerends LJ, van Driel PBAA, Baatenburg de Jong RJ,

et al. Real-time fluorescence imaging in intraoperative decision making for cancer surgery. Lancet Oncol 2021;22:e186-95.
6. Wu CY, Tai YJ, Shih IL, et al. Preoperative magnetic resonance imaging predicts clinicopathological parameters and stages of endometrial carcinomas. Cancer Med 2022;11:993-1004.
7. Pradipta AR, Tanei T, Morimoto K, et al. Emerging Technologies for Real-Time Intraoperative Margin Assessment in Future Breast-Conserving Surgery. Adv Sci (Weinh) 2020;7:1901519.
8. Pogue BW, Rosenthal EL. Review of successful pathways for regulatory approvals in open-field fluorescence-guided surgery. J Biomed Opt 2021;26:030901.
9. Lubner MG, Mankowski Gettle L, Kim DH, et al. Diagnostic and procedural intraoperative ultrasound: technique, tips and tricks for optimizing results. Br J Radiol 2021;94:20201406.
10. Osako T, Nishimura R, Nishiyama Y, et al. Efficacy of intraoperative entire-circumferential frozen section analysis of lumpectomy margins during breast-conserving surgery for breast cancer. Int J Clin Oncol 2015;20:1093-101.
11. St John ER, Al-Khudairi R, Ashrafian H, et al. Diagnostic Accuracy of Intraoperative Techniques for Margin Assessment in Breast Cancer Surgery: A Meta-analysis. Ann Surg 2017;265:300-10.
12. Landau MJ, Gould DJ, Patel KM. Advances in fluorescent-image guided surgery. Ann Transl Med 2016;4:392.
13. Gangadharan S, Sarkaria IN, Rice D, et al. Multiinstitutional Phase 2 Clinical Trial of Intraoperative Molecular Imaging of Lung Cancer. Ann Thorac Surg 2021;112:1150-9.
14. Azari F, Meijer RPJ, Kennedy GT, et al. Carcinoembryonic Antigen-Related Cell Adhesion Molecule Type 5 Receptor-Targeted Fluorescent Intraoperative Molecular Imaging Tracer for Lung Cancer: A Nonrandomized Controlled Trial. JAMA Netw Open 2023;6:e2252885.
15. Kennedy GT, Azari FS, Bernstein E, et al. Targeted Intraoperative Molecular Imaging for Localizing Nonpalpable Tumors and Quantifying Resection Margin Distances. JAMA Surg 2021;156:1043-50.
16. Bongsu J, Vullev VI, Anvari B. Revisiting indocyanine green: effects of serum and physiological temperature on absorption and fluorescence characteristics. IEEE Journal of Selected Topics in Quantum Electronics 2014;20:149-57.
17. Mordon S, Devoisselle JM, Soulie-Begu S, et al. Indocyanine green: physicochemical factors affecting its fluorescence in vivo. Microvasc Res 1998;55:146-52.
18. Li Y, You Q, Wang Z, et al. A study on setting standards for near-infrared fluorescence-image guided surgery (NIRFGS) time lapse monitoring based on preoperative liver function assessment. Ann Transl Med 2022;10:96.
19. Nairat M, Konar A, Kaniecki M, et al. Investigating the role of human serum albumin protein pocket on the excited state dynamics of indocyanine green using shaped femtosecond laser pulses. Phys Chem Chem Phys 2015;17:5872-7.
20. Saxena V, Sadoqi M, Shao J. Degradation kinetics of indocyanine green in aqueous solution. J Pharm Sci 2003;92:2090-7.
21. Jiang JX, Keating JJ, Jesus EM, et al. Optimization of the enhanced permeability and retention effect for near-infrared imaging of solid tumors with indocyanine green. Am J Nucl Med Mol Imaging 2015;5:390-400.
22. Kosaka N, Mitsunaga M, Longmire MR, et al. Near infrared fluorescence-guided real-time endoscopic detection of peritoneal ovarian cancer nodules using intravenously injected indocyanine green. Int J Cancer 2011;129:1671-7.
23. Madajewski B, Judy BF, Mouchli A, et al. Intraoperative near-infrared imaging of surgical wounds after tumor resections can detect residual disease. Clin Cancer Res 2012;18:5741-51.
24. Holt D, Okusanya O, Judy R, et al. Intraoperative near-infrared imaging can distinguish cancer from normal tissue but not inflammation. PLoS One 2014;9:e103342.
25. Bhavane R, Starosolski Z, Stupin I, et al. NIR-II fluorescence imaging using indocyanine green nanoparticles. Sci Rep 2018;8:14455.
26. von Roemeling C, Jiang W, Chan CK, et al. Breaking Down the Barriers to Precision Cancer Nanomedicine. Trends Biotechnol 2017;35:159-71.
27. Lin X, Liu C, Sheng Z, et al. Highly Sensitive Fluorescence and Photoacoustic Detection of Metastatic Breast Cancer in Mice Using Dual-Modal Nanoprobes. ACS Appl Mater Interfaces 2018;10:26064-74.
28. Kanazaki K, Sano K, Makino A, et al. Development of human serum albumin conjugated with near-infrared dye for photoacoustic tumor imaging. J Biomed Opt 2014;19:96002.
29. Wang Z, Chen M, Liu JJ, et al. Human Serum Albumin Decorated Indocyanine Green Improves Fluorescence-Guided Resection of Residual Lesions of Breast Cancer in Mice. Front Oncol 2021;11:614050.

30. Lim TH, Lai TYY, Takahashi K, et al. Comparison of Ranibizumab With or Without Verteporfin Photodynamic Therapy for Polypoidal Choroidal Vasculopathy: The EVEREST II Randomized Clinical Trial. JAMA Ophthalmol 2020;138:935-42.
31. Mieog JS, Troyan SL, Hutteman M, et al. Toward optimization of imaging system and lymphatic tracer for near-infrared fluorescent sentinel lymph node mapping in breast cancer. Ann Surg Oncol 2011;18:2483-91.
32. Philip R, Penzkofer A, Baumler W, et al. Absorption and fluorescence spectroscopic investigation of indocyanine green. Journal of Photochemistry and Photobiology A: Chemistry 1996;96:137-48.
33. Mauerer M, Penzkofer A, Zweck J. Dimerization, J-aggregation and J-disaggregation dynamics of indocyanine green in heavy water. Journal of Photochemistry and Photobiology B: Biology 1998;47:68-73.
34. Landsman ML, Kwant G, Mook GA, et al. Light-absorbing properties, stability, and spectral stabilization of indocyanine green. J Appl Physiol 1976;40:575-83.
35. Jang HJ, Song MG, Park CR, et al. Imaging of Indocyanine Green-Human Serum Albumin (ICG-HSA) Complex in Secreted Protein Acidic and Rich in Cysteine (SPARC)-Expressing Glioblastoma. Int J Mol Sci 2023;24:850.
36. Merlot AM, Kalinowski DS, Richardson DR. Unraveling the mysteries of serum albumin-more than just a serum protein. Front Physiol 2014;5:299.
37. Loureiro A, Azoia NG, Gomes AC, et al. Albumin-Based Nanodevices as Drug Carriers. Curr Pharm Des 2016;22:1371-90.
38. Watkins G, Douglas-Jones A, Bryce R, et al. Increased levels of SPARC (osteonectin) in human breast cancer tissues and its association with clinical outcomes. Prostaglandins Leukot Essent Fatty Acids 2005;72:267-72.
39. Hutteman M, Mieog JS, van der Vorst JR, et al. Randomized, double-blind comparison of indocyanine green with or without albumin premixing for near-infrared fluorescence imaging of sentinel lymph nodes in breast cancer patients. Breast Cancer Res Treat 2011;127:163-70.
40. Maeda H, Matsumura Y. EPR effect based drug design and clinical outlook for enhanced cancer chemotherapy. Adv Drug Deliv Rev 2011;63:129-30.
41. Torchilin V. Tumor delivery of macromolecular drugs based on the EPR effect. Adv Drug Deliv Rev 2011;63:131-5.

Cite this article as: Li Y, Dai C, Hua Z, Xia L, Ding Y, Wang Q, Gié MLM, Bouvet M, Cai H. A human serum albumin-indocyanine green complex offers improved tumor identification in fluorescence-guided surgery. Transl Cancer Res 2024;13(1):437-452. doi: 10.21037/tcr-23-2338

